Applied Physics A (2025) 131:610
https://doi.org/10.1007/s00339-025-08706-5

Dielectric characterization of the Al/p-Si structure with porous silicon wafer

Yashar Azizian-Kalandaragh[1,2,3] · **Yosef Badali**[4]

Received: 23 March 2025 / Accepted: 11 June 2025

Abstract
This study investigates the dielectric properties of aluminum/p-type silicon (Al/p-Si) structures modified by porous silicon (PS) layers formed via electrochemical etching. Porous silicon wafers were prepared under controlled current density conditions, and five distinct regions (P_1–P_5) were analyzed to assess local variations in surface morphology, chemical composition, and wettability. Surface characterization using energy-dispersive X-ray spectroscopy (EDX) and atomic force microscopy (AFM) revealed variations in oxygen content and porosity across the wafer, influencing wettability and dielectric behavior. Contact angle measurements demonstrated the combined effects of surface oxidation and pore size on hydrophilicity. Dielectric measurements showed that regions with higher porosity exhibited increased capacitance and dielectric constants, with frequency-dependent behavior attributed to interfacial polarization. These findings highlight the critical role of surface chemistry and morphology in tuning the dielectric response of PS-based devices. The enhanced dielectric properties of the Al/PS/p-Si structures suggest promising applications in microelectronics, biosensors, and energy storage technologies.

Keywords Schottky diode (SD) · Porous silicon (PS) · Electrochemical etching · Surface morphology · Wettability · Dielectric features

1 Introduction

Scientists and researchers have investigated the properties of silicon, a semiconductor material that is widely employed in many industries, in detail over the 20th and 21 st centuries [1–3]. Silicon can be synthesized in a variety of forms, sizes, and forms, such as wafer structures, quantum dots, and micro and nanostructures. Of them, the silicon wafer, which comes in two varieties known as p-type silicon (p-Si) wafer and n-type silicon (n-Si) wafer, is a useful structure type for creating new gadgets in contemporary technology [3–5]. It is a problem for researchers to engineer silicon wafer structures to become more effective. There are more than 2 degrees of freedom when it comes to processing silicon (for example creating undercut structures is also possible). Etching can change the thickness and the surface chemistry [5–7]. Since it is uncommon to alter the thickness of silicon wafers, scientists have looked at several methods to alter the physiochemical characteristics of the wafer surface. The silicon etching procedure, which leaves the silicon wafer with a porous surface, is one of these methods. Porous silicon (PS) has been recognized for its physical and chemical characteristics, and its applications include the fabrication of bioelectronics and biosensors, chemical and biological technology, the fabrication of gas sensors, and humidity sensors technology [7–10]. The structure of the PS layer is crucial in defining the accountability of the device on which the layer is based.

Therefore, silicon-based devices are the main structures to engineer the Si wafer. Significant attention has been directed

✉ Yashar Azizian-Kalandaragh
yashar.a.k@gmail.com

Yosef Badali
ybedeli@ticaret.edu.tr

1 Department of Photonics, Faculty of Applied Sciences, Gazi University, Ankara 06500, Türkiye

2 Photonics Application and Research Center, Gazi University, Ankara 06500, Türkiye

3 Department of Physics, University of Mohaghegh Ardabili, P.O. Box.179, Ardabil, Iran

4 Department of Computer Engineering, Istanbul Ticaret University, Istanbul 34445, Türkiye

Published online: 08 July 2025

recently toward addressing the key challenges concerning metal-semiconductor (MS) contacts or Schottky diodes (SDs) [11]. The primary objective has been to enhance the overall performance of these contacts. The structural characteristics of the fabricated device are strongly influenced by different factors, including the surface preparation techniques, the nature of the barrier height (BH) and interlayer materials at the M/S interface, the level of doping atoms, as well as the frequency, voltage, and temperature under which the devices operate [12]. These variables play a crucial role in determining the overall performance and effectiveness of MS contacts or SDs, making them essential considerations for further advancements and optimization in device design and functionality [13].

So, in the last five decades, especially semiconductor nanostructures have been given much attention because of their physical and chemical properties to improve their performance [14–16]. Among these inorganic materials (Si, Ge, GaAs, InP, CdS/CdTe), Si is one of the oldest and has low cost and high stability. Given its distinct characteristics, it finds utility across a wide spectrum of applications spanning numerous domains, with a pronounced presence in electronics and the fabrication technology of semiconductor devices, among others [16–19]. The unique characteristics of the Si are more evident when its dimensions are reduced. By reducing the size and dimension of Si, its physical and chemical properties change due to the quantum confinement effect [20, 21].

There are various methods used for the manipulation of Si nanostructures to change their physical properties such as doping by other materials [22], thermal annealing [23, 24], plasma treatment [25, 26], and electrochemical etching [27]. One of these types of manipulations is to create porosity in the Si surface called PS. PS is a dielectric material composed of silicon dioxide (SiO_2) and air, which has a structural heterogeneity much smaller than normal light wavelength [28]. Electrochemical etching is one of the most widely used methods for the surface treatment of Si wafers. In this method, the surface morphology of the samples has changed with the condition of the electrochemical etching [18, 19, 29]. The surface treatment contains the formation of porosity in the surface of the Si semiconductors that have different applications such as nonlinear optics [30], biology [31], solar cells (SCs) [32], and fabrication of Bragg-reflectors [33], microelectronics [34], waveguides [35], optical filter [36], gas sensors [37], photoluminescence devices in the visible region [38], energy [39], drug industry [40], biotechnology [41], and some other complex optical devices due to its high surface-to-volume ratio, high reactivity, luminescence properties at room temperature and its adaptive nature. There are several studies on the optical and structural applications of PS reported by researchers [28].

Wu et al. highlighted that superhydrophobic nickel surfaces provide superior corrosion protection compared to traditional methods that require toxic chemical inhibitors. While electrochemical etching is a useful technique for creating such surfaces, its effectiveness has been hindered by low current density and efficiency issues. To overcome these limitations, a novel wire electrochemical etching method was proposed, involving a controlled wire cathode in a NaCl electrolyte. This method successfully generated a superhydrophobic nickel surface with distinctive features such as a high contact angle and self-cleaning properties. By fine-tuning parameters and comprehending the formation of superhydrophobic surfaces, this approach has the potential to advance nickel corrosion protection technology by enhancing processing efficiency [19].

The findings of this study provide actionable insights for the design and fabrication of advanced silicon-based devices. By optimizing the electrochemical etching parameters to control porosity and surface oxidation, device engineers can tailor the dielectric properties of Al/p-Si structures for specific applications [42–44]. For instance, increasing porosity can enhance the capacitance and dielectric constant, which is beneficial for developing high-performance capacitors and sensors. Additionally, understanding the interplay between surface chemistry and wettability enables the creation of PS surfaces with tunable hydrophilicity or hydrophobicity, which is valuable for biosensing, lab-on-chip devices, and microfluidic platforms [45, 46]. The demonstrated methods can also be directly applied to improve the efficiency and reliability of Schottky diodes in microelectronics, as well as to engineer interfaces for energy storage and conversion systems such as supercapacitors and silicon-based batteries [47, 48].

In addition, the dielectric properties of the silicon-based SDs with/without an interlayer have been extensively investigated due to their importance in technological applications. The increase of the permittivity means an increase in the storage of electronic charges or energy, thus reducing many surface states (N_{ss}), series resistance (R_s), and dislocations [20]. Therefore, many investigations have been carried out to control the modification of electronic and transport properties of conventional MS-type SD structures by using various interlayers that have high-dielectric material to reduce leakage current, ideality factor, N_{ss}, R_s and thus enhance the device performance [49]. While previous studies have primarily focused on either the global properties of porous silicon or on specific device applications, few have systematically mapped the spatial variation of key surface and dielectric properties across a single wafer. Furthermore, the simultaneous influence of both oxidation and pore structure on wettability and dielectric response remains underexplored. Our work addresses these gaps by

providing a spatially resolved, multi-modal characterization of PS surfaces and directly linking these findings to device performance.

This study aims to investigate the structural, morphological, and wettability of etched surface p-Si and then examine the dielectric characteristics of the Al/p-Si SD at different points on the silicon surface with different porosity rates. First, the EDX and AFM analysis of the PS are performed. Second, the effect of the electrochemical etching process on the surface contact angle of the p-Si wafer is studied. Finally, the dielectric features such as complex permittivity ($\varepsilon^{'}$, $\varepsilon^{''}$), loss tangent (tanδ), and electrical modulus ($M^{'}$, $M^{''}$) for the Al/p-Si SD with porous Si wafer are calculated by measuring the frequency-dependent C and G parameters. The findings are thoroughly discussed.

2 Experimental details

For the preparation of PS, a 2-inch p-Si (100) oriented wafer ($\rho = 1–10\ \Omega$.cm), HF (50%) solution, distilled water, and ethanol (99.99%) were used. PS was prepared through the electrochemical etching of silicon in an HF solution, resulting in partial dissolution of Si. Various factors play a crucial role in governing this process, and it is essential to investigate and understand their influence. The choice of electrolyte is critical in PS formation. Typically, HF acid is utilized in concentrations up to 50% in distilled water. After rinsing the samples with ethanol to get rid of any debris, they were submerged in 50% HF acid for 15 min to get rid of any native oxide layer. To keep these samples submerged and preserved in a plastic container filled with methanol to stop the formation of an oxide layer on their surfaces once more, they were rinsed with ethanol again and then allowed to dry for a few minutes in the ambient atmosphere. Each sample was then fastened with a sheet serving as an anode and support material at the bottom of a Teflon singlet anodizing system. The cathode was a platinum mesh rod positioned 1 cm perpendicular to the Si surface. By changing the current density while maintaining a constant etching time, or vice versa, the final samples were produced. Several experiments were conducted to determine the best ratio for this work to approach the helpful solution mixture. To enhance the wettability of the PS surface and remove surface contaminants, ethanol was added to the solution. Ethanoic solutions infiltrate the pores effectively, leading to improved lateral homogeneity of the PS layer. Moreover, the presence of ethanol or other surfactants helps in the timely removal of hydrogen bubbles formed during the reaction, promoting a smoother surface.

The dissolution of silicon can be controlled by either regulating the anodic current or the potential. The constant current operation is generally preferred as it allows better control over the porosity, thickness, and reproducibility of the PS layer. The flow of current between the electrodes occurs through the Si wafer. HF circulation during the etching process aids in achieving good depth uniformity and is also advantageous from a safety standpoint. A lateral geometry for PS formation has been suggested recently, wherein a contact is deposited on the same surface where PS is formed [28]. This method promotes lateral rather than depth-wise PS formation, resulting in very flat PS/Si interfaces. Overall, understanding the various factors influencing the electrochemical etching process is crucial for obtaining uniform and high-quality PS layers with desirable properties for various applications.

After the electrochemical etching process was completed under constant conditions (current density of 10–50 mA/cm^2 for 15 min in 50% HF solution), five distinct regions were selected from different locations on the single PS wafer. These regions, labeled as P1 to P5, were chosen to assess the uniformity and local variations in porosity and surface properties across the wafer. All subsequent analyses (EDX, AFM, and contact angle measurements) were performed on these specific regions. Therefore, P1 to P5 do not correspond to samples prepared at different current densities, but rather to different areas on the same wafer etched under identical conditions.

The surface morphology and roughness measurement of the modified p-Si wafer were analyzed by Atomic Force Microscopy (AFM) model Nano Surf Core AFM (Switzerland). The contact angle was measured by a digital camera (Nikon model D7200) in ambient conditions at room temperature (25 °C). The water dropped onto the Si substrate from a Hamilton syringe.

After the electrochemical etching process, the wafer was thoroughly rinsed and dried. For dielectric property measurements, circular aluminum (Al) contacts (with a diameter of 1.2 mm) were thermally evaporated onto each of the five regions (P_1–P_5) using a shadow mask to define the contact area. The Al contacts served as the Schottky (rectifying) contacts, while the back side of the wafer was coated with a continuous Al layer to form an ohmic contact. The thickness of the Al contacts was approximately 60 nm, confirmed by a quartz crystal microbalance during deposition. The regions P_1–P_5 were selected from different locations across the wafer surface after etching, as described previously. Each region was individually contacted and measured to assess local variations in dielectric properties. The frequency-dependent capacitance (C-f) and conduction (G/ω-f) of the different regions of the sample have been measured by a KEYSIGHT impedance analyzer (E4980Al 20 Hz-1 MHz) at 25 ˚C. Dielectric measurements were attempted for all regions (P1–P5); however, due to technical issues with the

electrical contact on P1, reliable data could not be obtained for this region.

3 Results and discussion

3.1 Wettability measurement

Controlling the wettability of materials such as silicon or germanium, which are commonly used in optoelectronic devices, is important. Researchers have been competing to engineer substrates to increase or decrease the wettability of the surface [17]. Adding another material on the substrate is a known method for engineering the wettability of the surface, but it can also change the good properties (The features we require) of the device [50]. To overcome this problem, researchers have explored a new way of changing the morphology of the substrate physically or chemically, so that the porosity of the surface is one of them. Generally, the wettability of a surface is influenced by two key factors: the surface morphology or roughness and the surface composition or chemistry. Wettability, which is determined by the interaction of cohesive and adhesive forces, is the capacity of a liquid to spread and retain contact with a solid substrate surface. The liquid molecules interact with each other by Cohesive forces, which prevent the water droplet from touching the surface, while adhesive forces exist between the solid state and liquid, which make a liquid droplet spread over the surface [50]. The surface-liquid contact angle serves as a proxy for wettability features; an increase in contact angle corresponds with a decrease in wettability and vice versa. A contact angle of 180° degrees suggests that the liquid does not wet the surface, while a contact angle of zero degrees signifies that the liquid wets the entire surface. A surface is classified as hydrophilic if its contact angle is less than 90 degrees and as hydrophobic if it is greater than 90°. Measurements of contact angles are evaluated using the theories of Young, Wenzel, and Cassie-Baxter [50, 51]. A framework for calculating the contact angle of various surfaces with variable surface energy is provided by these theories. The equilibrium angle of smooth, chemically homogeneous surfaces can be computed using Young's theory. On the other hand, the contact angle of rough surfaces is determined using Wenzel's hypothesis. Wenzel's theory considers the roughness of the surface and corrects Young's equation accordingly. The Cassie-Baxter theory is used to measure the contact angle of surfaces with a composite of solid-air surfaces. This theory considers the air trapped in the surface grooves, which distinguishes it from Wenzel's theory [50, 51].

Therefore, the Young equation can be used to find the contact angle when a liquid drop comes into equilibrium in contact with a smooth solid surface, which is given by [51]:

$$Cos\theta = \frac{\gamma_{SV} - \gamma_{SL}}{\gamma_{LV}}, \tag{1}$$

where the θ denotes the contact angle, γ_{SV} is solid-vapor surface tension, γ_{SL} refers to solid-liquid surface tension, and γ_{LV} stands for liquid-vapor surface tension [51]. However, the equilibrium angle of rough surfaces cannot be determined using the Young equation. In this instance, the surface's roughness has an impact on how easily water droplets can cling to the surface. Young equation is employed for chemically homogenous surfaces, or smooth, stiff surfaces. However, non-ideal rough surfaces do not have complete chemical homogeneity, and the factors of chemical heterogeneity and roughness cannot be ignored. Both homogeneous and non-homogeneous rough textures are possible on a surface. When liquid fills the bumps on a rough surface, the state is known as homogenous wettability. Conversely, in cases where the surface is a mixture of two distinct materials or phases, non-homogeneous wettability arises [52–54]. The drop faces two distinct modes on rough surfaces. The first is the application of water droplets to every surface groove. In 1936, Wenzel presented the fundamental ideas of this situation [51]. According to Wenzel, the solid liquid's actual contact region beneath the drop is greater on a rough surface than it is on a smooth one. The rough surface gets wetter faster when the energy of the interface between solid and liquid is lower than the energy of the solid-air interface. This is because the system's energy falls as the roughness increases.

However, the surface refutes the intrinsic water when the energy of the solid-liquid contact is greater than that of the solid-air interface, making it extremely difficult for the rough surface to become wettable in this situation. Wenzel changed the Young equation and proposed the Wenzel equation, which is given by [55]:

$$Cos\theta_W = rCos\theta_Y, \tag{2}$$

where θ_w denotes the apparent angle according to Wenzel's theory, θ_Y represents the Yang equilibrium contact angle with a smooth surface for the same material, and r denotes the surface roughness ratio, which is determined by the equation given below [55]:

$$r = \frac{A_r}{A_0}. \tag{3}$$

The ratio of the real surface (A_r) to the geometric surface (A_0) is given by r [55]. Air gets trapped beneath the water drop and between the surface bumps if a drop of water is suspended on the rough surface, which is the second alternative [56]. These situations are known as Cassie-Baxter. An equation was proposed by Cassie and Baxter to investigate the liquid's contact angle on solid-air composite surface compounds. The Cassie-Baxter hypothesis differs from the Wenzel theory at these surfaces because air is trapped in the surface grooves. The Cassie-Baxter equation is given by [56]:

$$cos\theta_{cb} = 1 + f_{sl}(cos\theta_Y - 1). \quad (4)$$

where θ_{bc} is the contact angle based on Cassie-Baxter's theory, f_{sl} is a fraction of solid-liquid surface area, and θ_Y is the Yang angle. In comparison to the Wenzel model, this model displays a more accurate system; yet it is challenging to estimate parameters effectively for surfaces that have unpredictable roughness [56].

Figure 1 shows the contact angle measurements of water droplets on the p-Si wafer surface at different points of P_1 to P_5. As can be seen, the value of the contact angle decreases by increasing the porosity rate from the region P_1 to P_5. The contact angle is nearly 33° at the P_1 region, which continuously decreases with the increase of the porosity; at last, it reaches about 17°. It indicates the surface of the p-Si wafer is becoming hydrophilic by growing the porosity. Based on the photo taken from different regions of the p-Si wafer, there is indeed a change in wettability properties from P_1 to P_5, however, it is insignificant.

To determine which wetting regime applies to each region, we compared the measured contact angles with the predictions of the Wenzel and Cassie-Baxter models. For regions with higher contact angles (more hydrophobic), such as P_1 and P_2, the Cassie-Baxter model is more applicable, suggesting that air pockets are trapped beneath the droplet. In contrast, for regions like P_4 and P_5, which exhibited a lower contact angle and thus more hydrophilic behavior, the Wenzel model is more appropriate. This indicates that the water droplet penetrates into the surface roughness and pores, consistent with a pore-filling regime. These findings are supported by the observed surface morphologies from AFM (in the next part), which show increased roughness and porosity in the P_5 region.

3.1.1 Distinguishing the effects of oxidation and pore size on wettability

In our study, we acknowledge that both surface oxidation and pore size can significantly influence the wettability of porous silicon. To address this, we analyzed the correlation between oxygen content (as determined by EDX in the next section) and contact angle measurements for different regions (P_1–P_5). By comparing these data, we could identify regions where changes in wettability were more closely associated with oxidation levels, independent of substantial pore size variation.

Additionally, we utilized theoretical models (Wenzel and Cassie-Baxter) to interpret the contact angle data. The Wenzel model emphasizes the role of surface roughness (related to pore size), while deviations from this model may indicate chemical heterogeneity, such as differences in surface oxidation. This combined approach allowed us to qualitatively distinguish the contributions of surface chemistry and morphology to the overall wettability behavior.

While both factors are interrelated and can influence each other, our analysis suggests that regions with higher

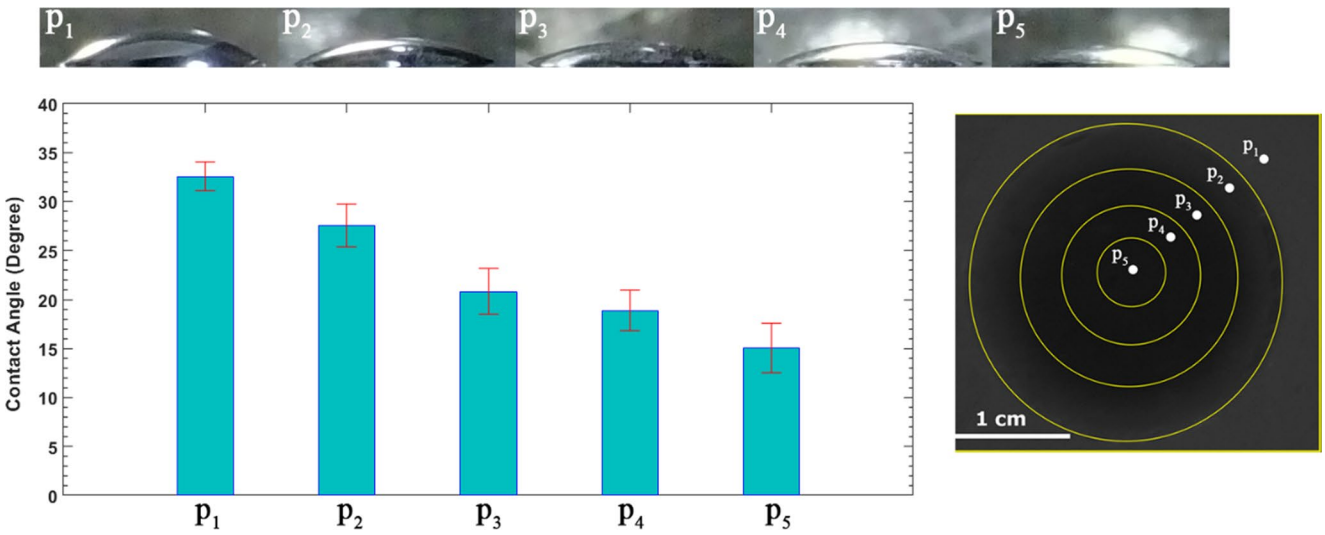

Fig. 1 Water drops on the p-Si wafer surface in different points P_1 to P_5 and their corresponding contact angle

oxidation (as indicated by EDX) tend to exhibit increased hydrophilicity, whereas regions with larger pore sizes and roughness generally show enhanced hydrophobicity, as predicted by the Wenzel and Cassie-Baxter models.

3.2 EDX & AFM analysis

Table 1. introduces the EDX results of the PS in different regions (P_1 to P_5) with varying porosity rates. This elemental analysis reveals that the increase in the electrochemical etching operation led to a significant increase in the presence of oxygen in the relevant areas. This finding indicates that the chemistry of the sample surface has significantly changed, resulting in a change in the ratio of silicon to oxygen.

The EDX analysis revealed that the central regions of the PS wafer, which experienced higher etching rates, exhibited a noticeably higher oxygen content compared to the outer regions. This observation can be attributed to the increased surface-to-volume ratio in these areas, which makes them more prone to native oxidation once the etching process is completed. The larger exposed surface area in the highly etched regions facilitates more rapid and extensive oxidation when exposed to ambient conditions, resulting in the higher oxygen concentrations detected by EDX.

An analysis of different regions of the etched areas on the p-Si surface using AFM is investigated. The analysis is conducted in the radial direction of different areas, which are illustrated in the image and numbered from P_1 to P_5. Figure 2 depicts the AFM images of different points (P_1 to P_5) in the radial directions of the electrochemically etched p-Si wafer. A comparative analysis of the surface from AFM images revealed high surface roughness in the unetched region (Fig. 2-P1), while smoother surfaces were observed in the inner layer of the circle.

In other words, the spot created by electrochemical etching contained different areas, with the surface roughness being high in the outer rings and decreasing in the inner rings and center. To further quantify the observed differences in surface morphology, Table 2 presents the pore size values at different points on p-Si. The results indicate that the diameter and depth of the etched region increased with increasing distance from the center of the circle. Additionally, the mean pore size of the etched region was found to be highest at the center and decreased towards the outer rings, as shown in Table 2. While AFM imaging provides valuable insights into the nanoscale surface texture of the porous silicon regions (P_1–P_5), it is challenging to determine individual pore sizes accurately due to the interconnected and highly porous nature of the structure. Instead, we focus on a qualitative assessment of surface roughness: the AFM images reveal pronounced variations in roughness across different regions, with denser distributions of protrusions and depressions indicating higher porosity and increased surface area. These morphological differences are consistent with the observed variations in wettability and dielectric properties. Thus, our analysis emphasizes qualitative roughness comparisons rather than unreliable quantitative pore size extraction from AFM data.

Table 1 The EDX results in both atomic and weight percentages

Elements				
Region	Atomic %		Wt %	
	Oxygen	Silicon	Oxygen	Silicon
P_1	16.68	83.32	10.24	89.76
P_2	20.37	79.63	12.72	87.28
P_3	24.71	75.29	15.75	84.25
P_4	26.61	73.39	17.12	82.88
P_5	26.04	73.96	16.71	83.29

3.3 Dielectric characteristics

The imaginary constituents of complex impedance, comprising the values of C and G/ω, were harnessed to compute parameters such as ε', ε'', and tanδ, representing the ratio of ε' to ε'', as well as the electric modulus ($M^* = M' + jM''$) across a frequency range spanning from 0.1 kHz to 1 MHz in the applied voltage of 1.5 V. The profiles of C-f and G/ω-f for the entire PS region are illustrated in Fig. 3(a) and 3(b) respectively. Dielectric property data for the P1 region could not be obtained due to technical issues with electrical contact during measurement. Only reliable data for P2–P5 are reported in this study. Notably, both C and G/ω display a robust dependence on frequency, exhibiting a consistent reduction as the frequency escalates. The augmented values of C and G/ω at lower frequencies are linked to the augmented capacitance and conductance attributed to the presence of surface states (N_{ss}). This arises as N_{ss} readily responds to the AC signal at lower frequencies, significantly contributing to the measured capacitance of the SD. However, at higher frequencies, the influence of N_{ss} diminishes, as they struggle to trace the AC signal. Intriguingly, augmenting the intensity of the etching process yields amplified values of both C and G/ω.

The amount of ε', ε'', and tan(δ) are characterized by C-f and G/ω-f behavior in the range 0.1 kHz to 1 MHz by using the following relations [57]:

$$\epsilon^* = \epsilon' - j\epsilon'' = \frac{C}{C_0} - j\frac{G}{\omega C_0} \tag{5}$$

$$tan\delta = \frac{\epsilon''}{\epsilon'} \tag{6}$$

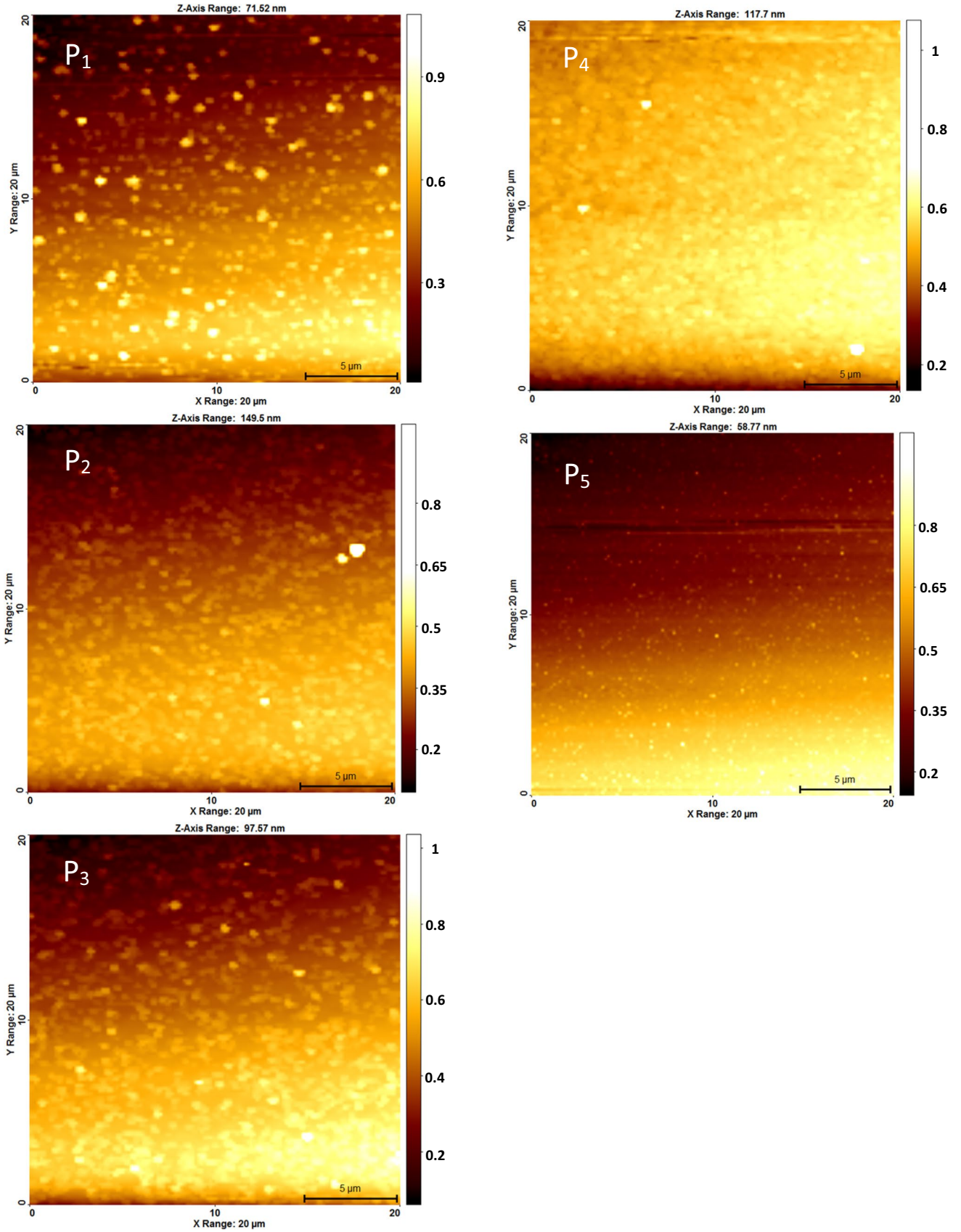

Fig. 2 AFM images of different points (P1 to P5) in the radial difference of the electrochemically etched p-Si wafer

Table 2 The pore size in different regions on the p-Si surface

Region	P_1	P_2	P_3	P_4	P_5
size (nm)	4.179	3.406	3.252	2.63	1.239

Here, C_0 represents the geometry capacitance as ($=\varepsilon_0 A/d$), served as a reference. The frequency-dependent variations of ε' and ε'' as well as tanδ parameters are illustrated in Figs. 4(a-c).

Experimental findings revealed that both ε' and ε'' are highly dependent on frequency, mirroring the behavior observed in C-f and G-f plots. As shown in Figs. 4(a, b), at low frequencies, both the ε' and ε'' decrease with increasing frequency, while at high frequencies, these values remain relatively constant. This phenomenon can be attributed to the increasing influence of the series resistance (R_s) of the MS-type SD at higher frequencies, whereas at lower frequencies, both the surface state density (N_{ss}) and polarization effects play more significant roles. These observed results are consistent with similar behaviors reported in different materials [57].

The reason for the dispersive behavior of ε' and ε'' at low and intermediate frequencies is due to various factors, such as Maxwell-Wagner relaxation, dipole/surface polarizations, N_{ss}, and the native interfacial insulator layer. When the frequency decreases, ε' and ε'' increase, indicating that dipoles have enough time to align with the alternating electric field. The Maxwell-Wagner relaxation is connected to uncompensated surface charges at the capacitor's interface. At very high frequencies (≥10 GHz), electronic and ionic polarizations may occur, but at lower frequencies up to a few kHz, dipole and surface polarizations are observed [58]. In this study, measurements have been taken in the frequency range of 0.1 kHz-1 MHz, where electronic and ionic polarizations did not significantly influence the results. Figure 4(c) shows a distinct peak in tanδ plots of different regions of P_2-P_5 at a frequency near 50 kHz, especially at

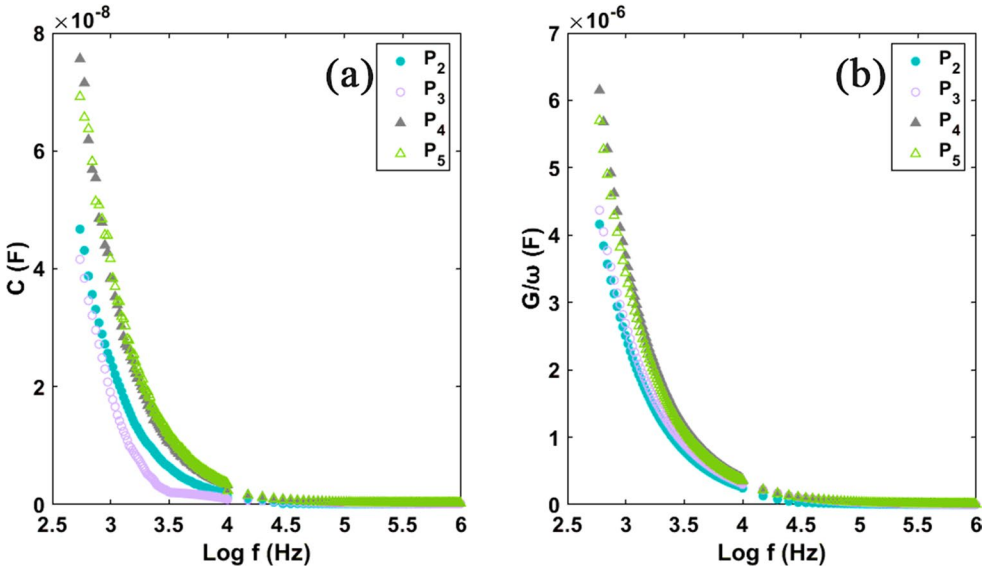

Fig. 3 The plots of (a) C-f and (b) G/ω-f characteristics for different regions of PS (P_2 to P_5)

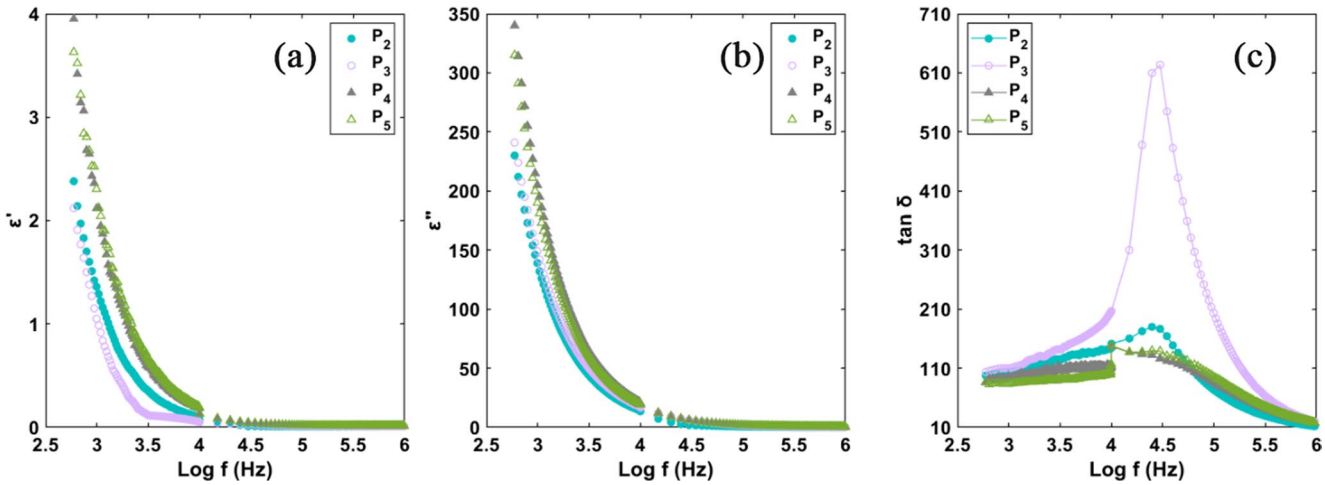

Fig. 4 The plots of (a) ε'-f, (b) ε''-f, and (c) tan(δ)-f for different regions of PS (P_2 to P_5)

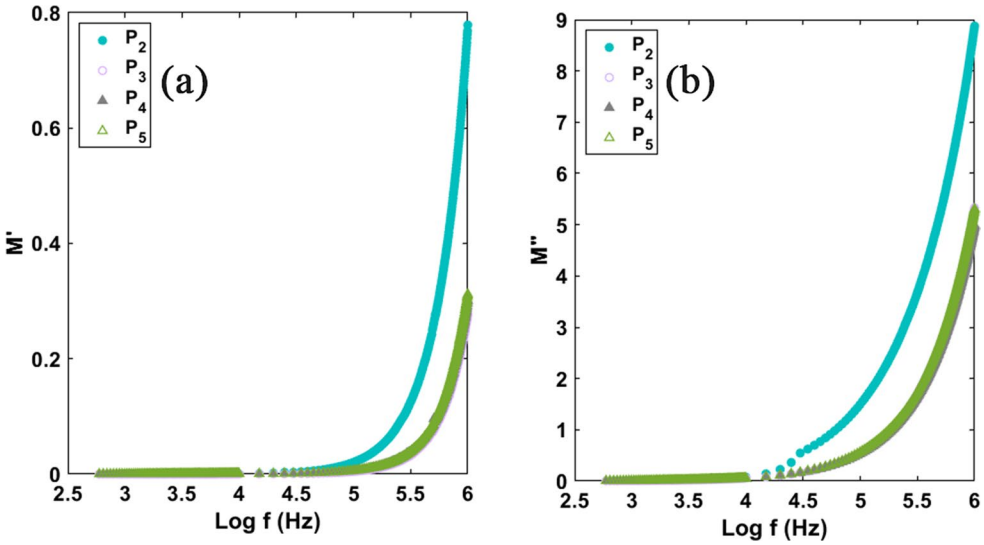

Fig. 5 The plots of a) M'-f and b) M"-f for different regions of PS (P_2 to P_5)

P_2 and P_3 regions. The presence of grains and grain boundaries can lead to increased resistance at lower frequencies. Additionally, grain resistance diminishes as frequency increases. Nevertheless, higher levels of electrical energy are needed to facilitate the movement of charge carriers at lower frequencies, and conversely. These are attributed to the decreasing tanδ values with respect to frequency. It must be noted that the observed similarity in dielectric properties between regions P_2 and P_3, as well as between P_4 and P_5, can be attributed to their comparable porosity and surface morphology, as indicated by AFM and EDX analyses. These regions likely experienced similar etching conditions, resulting in analogous microstructural features that influence their dielectric behavior.

By transformation of the permittivity into modulus data, complex dielectric modulus can be found as [58]:

$$M^* = \frac{1}{\epsilon^*} = M' + jM'' = \frac{\epsilon'}{\epsilon'^2 + \epsilon''^2} + j\frac{\epsilon''}{\epsilon'^2 + \epsilon''^2} \quad (7)$$

Figure 5(a, b) represents the double logarithmic M'-f and M"-f plots for all regions of PS with different porosity rates. The data depicted in Fig. 5 indicates that both the real part (M') and the imaginary part (M") of the material's complex electric module increase as the frequency rises, primarily due to a reduction in polarization effects. However, at higher frequencies, each applied forward bias voltage leads to the attainment of a maximum value for M' and M", corresponding to $M_\infty = 1/\varepsilon_\infty$ [59]. This behavior is a consequence of relaxation processes.

The significant augmentation in M' with increasing frequency can be attributed to the short-range mobility of charge carriers, which results in a lack of restoring force for the flow of charges under the influence of a steady electric field. Furthermore, the conduction mechanism may be predominantly governed by the hopping of carriers between surface states. In essence, the conductivity can be regarded as an electric field-activated hopping process, where charges move from one trap to another [60].

The variation in dielectric properties across different regions of the PS wafer is closely related to differences in porosity. Higher porosity generally increases the dielectric constant and capacitance, due to the larger effective surface area and the enhanced contribution of the porous network to charge storage. Additionally, regions with higher porosity may exhibit more pronounced frequency dispersion in dielectric properties, likely due to increased interfacial polarization. This trend is consistent with our observations for regions (specify regions, e.g., P_4 and P_5), which display both higher porosity and higher dielectric constants compared to less porous regions.

4 Conclusions

In this work, we systematically investigated the influence of electrochemical etching on the surface properties and dielectric behavior of Al/p-Si structures with porous silicon (PS) layers. By analyzing five distinct regions (P_1–P_5) across the PS wafer, we demonstrated that electrochemical etching leads to significant spatial variations in both surface chemistry and morphology, as revealed by EDX and AFM analyses. Our results showed that the central regions, which experienced higher etching rates, exhibited increased surface-to-volume ratios and consequently higher oxygen content due to enhanced native oxidation.

Wettability measurements indicated that both surface oxidation and pore size play critical roles in determining the hydrophilic or hydrophobic nature of the PS surface. Regions with higher oxygen content tended to be more

hydrophilic, consistent with the Wenzel wetting regime, where water droplets penetrate the porous structure. In contrast, regions with larger pore sizes and lower oxidation sometimes displayed more hydrophobic behavior, which could be described by the Cassie-Baxter model. This dual influence underscores the importance of considering both surface chemistry and morphology when engineering the wettability of PS surfaces for specific applications.

Dielectric characterization of the Al/PS/p-Si structures revealed that regions with higher porosity and oxidation exhibited enhanced dielectric constants and capacitance values, particularly at lower frequencies. This behavior is attributed to increased interfacial polarization and the larger effective surface area provided by the porous network. The observed frequency dependence of the dielectric properties further highlights the tunability of PS-based devices through careful control of etching parameters.

Despite some limitations, such as the unavailability of dielectric data for the P1 region and the lack of high-resolution AFM images, the study provides valuable insights into the interplay between surface treatment, morphology, chemistry, and electrical properties in PS systems. These findings have practical implications for the design and optimization of microelectronic devices, sensors, and energy storage components, where tailored dielectric and wetting properties are crucial.

In summary, our results demonstrate that electrochemical etching is an effective and versatile method for tuning the surface and dielectric properties of p-Si wafers. By optimizing etching conditions, it is possible to engineer PS surfaces with desirable characteristics for a wide range of technological applications, including microelectronics, biosensing, and energy conversion. Future work will focus on further refining surface characterization techniques and expanding the range of electrical measurements to fully exploit the potential of porous silicon in advanced device architectures.

Author contributions The author's contributions to this paper are as follows: Yashar Azizian-Kalandaragh, Experiments, Data analyses, writing, editing, and discussion; Yosef Badali, Discussion, Writing, and editing.

Funding Not applicable.

Data availability The data that support the findings of this study are available from the corresponding author upon reasonable request.

Declarations

Compliance with ethical standards Not applicable.

Consent for publication Not applicable.

Consent to participate Not applicable.

Conflict of interest The authors declare no financial or commercial conflict of interest.

References

1. D.J. DiMaria, J. Kirtley, E. Pakulis, D. Dong, T. Kuan, F. Pesavento, T. Theis, J. Cutro, S. Brorson, Electroluminescence studies in silicon dioxide films containing tiny silicon Islands. J. Appl. Phys. **56**, 401–416 (1984)
2. L.S. Ramsdell, Studies on silicon carbide, American mineralogist. J. Earth Planet. Mater. **32**, 64–82 (1947)
3. A. Shiohara, S. Prabakar, A. Faramus, C.-Y. Hsu, P.-S. Lai, P.T. Northcote, R.D. Tilley, Sized controlled synthesis, purification, and cell studies with silicon quantum Dots. Nanoscale. **3**, 3364–3370 (2011)
4. J. Sha, J. Niu, X. Ma, J. Xu, X. Zhang, Q. Yang, D. Yang, Silicon nanotubes. Adv. Mater. **14**, 1219–1221 (2002)
5. B. Ravi, O. Omotoye, T. Srivatsan, M. Petrorali, T. Sudarshan, The microstructure and hardness of silicon carbide synthesized by plasma pressure compaction. J. Alloys Compd. **299**, 292–296 (2000)
6. T.M. Atkins, A. Thibert, D.S. Larsen, S. Dey, N.D. Browning, S.M. Kauzlarich, Femtosecond ligand/core dynamics of microwave-assisted synthesized silicon quantum Dots in aqueous solution. J. Am. Chem. Soc. **133**, 20664–20667 (2011)
7. L.A. Field, P.P. Merchant, Fabrication of single-crystal silicon structures using sacrificial-layer wafer bonding. in, Google Pat. (1999)
8. S. Noh, X. Hao, Z. Liu, M.A. Green, S. Lee, A. Ho-Baillie, Investigating the effect of silicon thickness on ultra-thin silicon on insulator as a compliant substrate for gallium arsenide heteroepitaxial growth. Thin Solid Films. **653**, 371–376 (2018)
9. K. Sato, M. Shikida, Y. Matsushima, T. Yamashiro, K. Asaumi, Y. Iriye, M. Yamamoto, Characterization of orientation-dependent etching properties of single-crystal silicon: effects of KOH concentration. Sens. Actuators A: Phys. **64**, 87–93 (1998)
10. N.K. Ingle, A. Wang, Z. Li, M. Korolik, Methods for selective etching of a silicon material using HF gas without nitrogen etchants. in, Google Pat. (201)9
11. H. Sharma, S.N. Sharma, G. Singh, S. Shivaprasad, Effect of ratios of cd: se in CdSe nanoparticles on optical edge shifts and photoluminescence properties. Phys. E: Low-dimensional Syst. Nanostruct. **31**, 180–186 (2006)
12. S. Baskoutas, A.F. Terzis, Size-dependent band gap of colloidal quantum Dots. J. Appl. Phys. **99**, 013708 (2006)
13. S. Kolahi, S. Farjami-Shayesteh, Y. Azizian-Kalandaragh, Comparative studies on energy-dependence of reduced effective mass in quantum confined ZnS semiconductor nanocrystals prepared in a polymer matrix. Mater. Sci. Semiconduct. Process. **14**, 294–301 (2011)
14. U. Woggon, *Optical properties of semiconductor quantum dots* (Springer, 1997)
15. S. Altindal, J. Farazin, G. Pirgholi-Givi, E. Maril, Y. Azizian-Kalandaragh, The effects of (Bi2Te3–Bi2O3-TeO2-PVP) interfacial film on the dielectric and electrical features of Al/p-Si (MS) Schottky barrier diodes (SBDs). Phys. B: Condens. Matter. **582**, 411958 (2020)
16. Y. Azizian-Kalandaragh, İ. Yücedağ, G. Ersöz Demir, Ş. Altındal, Investigation of the variation of dielectric properties by applying frequency and voltage to Al/(CdS-PVA)/p-Si structures. J. Mol. Struct. **12**, 129325 (2021)
17. J. Farazin, G. Pirgholi-Givi, Y. Azizian-Kalandaragh, Wettability measurement, optical characteristics, and investigation of the quantum confinement effect of ZnS-scotch tape nanocomposite

films prepared by successive ionic layer adsorption and reaction (SILAR) method. Phys. B: Condens. Matter. **564**, 94–103 (2019)
18. H. Kudo, T. Sawada, E. Kazawa, H. Yoshida, Y. Iwasaki, K. Mitsubayashi, A flexible and wearable glucose sensor based on functional polymers with Soft-MEMS techniques. Biosens. Bioelectron. **22**, 558–562 (2006)
19. B. Wu, D. Yan, J. Lin, J. Song, Wire Electrochemical Etching of Superhydrophobic Nickel Surfaces with Enhanced Corrosion Protection, Materials **16,** 7472 (2023)
20. V. Lehmann, U. Gösele, Porous silicon formation: A quantum wire effect. Appl. Phys. Lett. **58**, 856–858 (1991)
21. X. Tang, G. Wen, Y. Song, Stable silicon/3D porous N-doped graphene composite for lithium-ion battery anodes with self-assembly. Appl. Surf. Sci. **436**, 398–404 (2018)
22. A. Lyuleeva, P. Holzmüller, T. Helbich, M. Stutzmann, M.S. Brandt, M. Becherer, P. Lugli, B. Rieger, Charge transfer doping in functionalized silicon nanosheets/P3HT hybrid material for applications in electrolyte-gated field-effect transistors. J. Mater. Chem. C **6**, 7343–7352 (2018)
23. B. Macco, J. Melskens, N.J. Podraza, K. Arts, C. Pugh, O. Thomas, W.M. Kessels, Correlating the silicon surface passivation to the nanostructure of low-temperature a-Si H after rapid thermal annealing. J. Appl. Phys. **122**, 035302 (2017)
24. M. Kim, M. Abbott, N. Nampalli, S. Wenham, B. Stefani, B. Hallam, Modulating the extent of fast and slow boron-oxygen related degradation in Czochralski silicon by thermal annealing: evidence of a single defect. J. Appl. Phys. **121**, 053106 (2017)
25. M. Wiegand, M. Reiche, U. Gösele, Time-Dependent surface properties, and wafer bonding of O 2-Plasma-Treated silicon (100) surfaces. J. Electrochem. Soc. **147**, 2734–2740 (2000)
26. A. Descoeudres, L. Barraud, S. De Wolf, B. Strahm, D. Lachenal, C. Guérin, Z. Holman, F. Zicarelli, B. Demaurex, J. Seif, Improved amorphous/crystalline silicon interface passivation by hydrogen plasma treatment. Appl. Phys. Lett. **99**, 123506 (2011)
27. O. Bisi, S. Ossicini, L. Pavesi, Porous silicon: a quantum sponge structure for silicon based optoelectronics. Surf. Sci. Rep. **38**, 1–126 (2000)
28. A. Barkhordari, S. Özçelik, Ş. Altındal, G. Pirgholi-Givi, H. Mashayekhi, Y. Azizian-Kalandaragh, The effect of PVP: BaTiO3 interlayer on the conduction mechanism and electrical properties at MPS structures. Phys. Scr. **96**, 085805 (2021)
29. L.T. Canham, *Properties of porous silicon,* (Institution of Electrical Engineers, 1997)
30. C.J. Oton, M. Ghulinyan, Z. Gaburro, P. Bettotti, L. Pavesi, L. Pancheri, S. Gialanella, N. Capuj, Scattering rings as a tool for birefringence measurements in porous silicon. J. Appl. Phys. **94**, 6334–6340 (2003)
31. V. Agarwal, J. Del, Rıo, Tailoring the photonic band gap of a porous silicon dielectric mirror. Appl. Phys. Lett. **82**, 1512–1514 (2003)
32. P. Yang, R. Yan, M. Fardy, Semiconductor nanowire: what's next? Nano Letter. **10**, 1529–1536 (2010)
33. P. Ferrand, R. Romestain, J. Vial, Photonic band-gap properties of a porous silicon periodic planar waveguide. Phys. Rev. B **63**, 115106 (2001)
34. Y. Azizian-Kalandaragh, M.B. Muradov, R.K. Mamedov, M. Behboudnia, A. Khodayari, Structural, compositional and optical characterization of water-soluble cds nanoparticles synthesized by ultrasonic irradiation. J. Optoelectron. Adv. Mater. Rapid Commun. **2**(1), 42 (2008)
35. L. Pavesi, C. Mazzoleni, A. Tredicucci, V. Pellegrini, Controlled photon emission in porous silicon microcavities. Appl. Phys. Lett. **67**, 3280–3282 (1995)
36. Y. Zhou, P. Snow, P.S.J. Russell, Strong modification of photoluminescence in erbium-doped porous silicon microcavities. Appl. Phys. Lett. **77**, 2440–2442 (2000)
37. R. Dubey, D. Gautam, Fabrication and characterization of porous silicon layers for applications in optoelectronics. Opt. Quantum Electron. **41**, 189 (2009)
38. P. Calcott, K. Nash, L. Canham, M. Kane, D. Brumhead, Identification of radiative transitions in highly porous silicon. J. Phys.: Condens. Matter. **5**, L91 (1993)
39. G. Barillaro, A. Diligenti, F. Pieri, F. Fuso, M. Allegrini, Integrated porous-silicon light-emitting diodes: a fabrication process using graded doping profiles. Appl. Phys. Lett. **78**, 4154–4156 (2001)
40. S. Dhanekar, S. Jain, Porous silicon biosensor: current status. Biosens. Bioelectron., 54–64 (2013)
41. H. Föll, M. Christophersen, J. Carstensen, G. Hasse, Formation and application of porous silicon. Mater. Sci. Engineering: R: Rep. **39**, 93–141 (2002)
42. D.I. Tishkevich, A.I. Vorobjova, D. Vinnik, Formation and corrosion behavior of nickel/alumina nanocomposites. Solid State Phenom. **299**, 100–106 (2020)
43. D.I. Tishkevich, A.I. Vorobjova, A.V. Trukhanov, Thermal stability of nano-crystalline nickel electrodeposited into porous alumina. Solid State Phenom. **299**, 281–286 (2020)
44. D.L. Shimanovich, A.I. Vorobjova, D.I. Tishkevich, A.V. Trukhanov, M.V. Zdorovets, A.L. Kozlovskiy, Preparation and morphology-dependent wettability of porous alumina membranes. Beilstein J. Nanotechnol. **9**, 1423–1436 (2018)
45. D.I. Tishkevich, A.I. Vorobjova, D. Vinnik, Template assisted Ni nanowires fabrication. Mater. Sci. Forum. **946**, 235–241 (2019)
46. Y. Badali, Y. Azizian-Kalandaragh, The influence of the physicochemical processes on the electrical response of Al/p-Si structure with etched surface. Appl. Phys. A **130**, 243 (2024)
47. A. Barkhordari, Ş. Altındal, S. Özçelik, H.R. Mashayekhi, M. Muradov, Y. Azizian-Kalandaragh, Enhancement of the optoelectric and photovoltaic responses of al/pvp: ZnTiO3/p-Si structure by graphene nanoparticles. Adv. Photonics Res., 2400171 (2025)
48. Y. Azizian-Kalandaragh, A. Barkhordari, Y. Badali, Support vector machine for prediction of the electronic factors of a Schottky configuration interlaid with pure PVC and doped by Sm2O3 nanoparticles. Adv. Electron. Mater., 2400624 (2024)
49. S.M. Sze, *Semiconductor devices: physics and technology* (Wiley, 2008)
50. D. Bonn, J. Eggers, J. Indekeu, J. Meunier, E. Rolley, Wetting and spreading, Reviews of modern physics, **81**, 739 (2009)
51. G. Kumar, K.N. Prabhu, Review of non-reactive and reactive wetting of liquids on surfaces. Adv. Colloid Interface Sci. **133**, 61–89 (2007)
52. Y. Azizian-Kalandaragh, Preparation of lead oxide nanostructures in presence of Polyvinyl alcohol (PVA) as capping agent and investigation of their structural and optical properties. J. Semicond. Technol. Sci. **18**(1), 91–99 (2018)
53. K. Liu, X. Yao, L. Jiang, Recent developments in bio-inspired special wettability. Chem. Soc. Rev. **39**, 3240–3255 (2010)
54. A.M. Mohamed, A.M. Abdullah, N.A. Younan, Corrosion behavior of superhydrophobic surfaces: A review. Arab. J. Chem. **8**, 749–765 (2015)
55. A. Marmur, Wetting on hydrophobic rough surfaces: to be heterogeneous or not to be? Langmuir, **19**, 8343–8348 (2003)
56. A. Razzaghi, M. Maleki, Y. Azizian-Kalandaragh, The influence of post-annealing treatment on the wettability of Ag+/Na+ ion-exchanged soda-lime glasses. Appl. Surf. Sci. **270**, 604–610 (2013)
57. Y. Azizian-Kalandaragh, Impedance spectroscopy (IS) and thermally stimulated discharged current (TSDC) studies on CdSe-PVA nanocomposites prepared by ultrasound-assisted method. Optoelectron. Adv. Mater. Rapid Commun., **4**(2) (2010)
58. Ş. Altındal, A. Barkhordari, Y. Azizian-Kalandaragh, B.S. Çevrimli, H.R. Mashayekhi, Dielectric properties and

negative-capacitance/dielectric in Au/n-Si structures with PVC and (PVC: Sm2O3) interlayer. Mater. Sci. Semiconduct. Process. **147**, 106754 (2022)
59. N. Hamdaoui, Y. Azizian-Kalandaragh, B. Zaidi, A. Ahmed, Akl, Evolution of microstructure, strain and physical properties of quaternary nanoparticles La0.8−xCexAg0.2MnO3 perovskites, applied physics A. Mater. Sci. Process. **127**, 1–18 (2021)
60. A. Barkhordari, Ş. Altındal, G. Pirgholi-Givi, H. Mashayekhi, S. Özçelik, Y. Azizian-Kalandaragh, The influence of PVC and (PVC: SnS) interfacial polymer layers on the electric and dielectric properties of Au/n-Si structure, Silicon, **15**, 855–865 (2023)